Journal of Sound and Vibration (1999) **226**(4), 675–700
Article No. jsvi.1999.2317, available online at http://www.idealibrary.com on IDEAL®

FINITE DIFFERENCING METHODS FOR THE MEASUREMENT OF DYNAMIC BENDING STRAIN

D. G. KARCZUB AND M. P. NORTON

Department of Mechanical and Materials Engineering, Centre for Acoustics, Dynamics and Vibration, The University of Western Australia, Nedlands, WA, 6907, Australia

(*Received* 5 *February* 1998, *and in final form* 31 *March* 1999)

Finite differencing formulations for dynamic bending strain are used to define measurement methods for autospectral, spatial and time history predictions of dynamic bending strain. These measurement methods provide predictions of dynamic bending strain in both nearfield and farfield regions from discrete measurements of displacement, velocity or acceleration. The differencing formulations considered use either three- or four-point finite differencing requiring simultaneous measurements at three or four positions, respectively. The number of simultaneous measurements required is reduced to two if the response is stationary and frequency response methods are used. The main limitation of these differencing methods is that the spatial extent of the measurement array precludes the prediction of dynamic bending strain at locations such as a clamped boundary where dynamic strain is usually largest. Experimental results are presented demonstrating autospectral, spatial and time history predictions of dynamic strain in both nearfield and farfield regions, and sources of errors in predictions are discussed. As structural intensity is given by the product of dynamic stress and velocity, the work presented here is also of interest for structural intensity measurements, particularly in nearfield regions when evanescent waves cannot be neglected.

© 1999 Academic Press

1. INTRODUCTION

Measurement methods for the estimation of dynamic stress utilizing portable accelerometers in place of strain gauges are of interest for assessing the fatigue life of randomly vibrating structures. Benefits of using accelerometers in place of strain gauges are summarized in Karczub [1]. The objective of the present work is to investigate the application of finite differencing methods, developed for structural intensity measurements, to the measurement of dynamic stress in randomly vibrating structures. The motivation for extending structural intensity finite differencing techniques to the measurement of dynamic stress stems from the definition of structural intensity in terms of the product of dynamic stress and velocity. Finite differencing methods for the measurement of dynamic stress are also investigated here as an alternative to the use of correlations between dynamic

0022–460X/99/390615 + 26 $30.00/0 © 1999 Academic Press

stress and velocity [1] which only provide exact autospectral and time history predictions of dynamic stress in farfield regions.

The formulations developed in this paper provide direct measurements of dynamic stress autospectra and time histories at a point in both nearfield and farfield regions. The derivations of these formulations are based on similar derivations for structural intensity measurement methods presented by Pavic [2], Verheij [3], Cuschieri [4] and Linjama and Lahti [5]. Equations are also derived to correct for finite differencing errors associated with propagating and evanescent waves. The predictions are exact in farfield regions once corrected for propagating wave finite differencing errors, and are slightly conservative in nearfield regions. The experimental analysis presented for autospectral, spatial and time history predictions considers the accuracy of predictions with frequency, the effects of transducer spacing, whether dynamic stress is correctly predicted in the near field and far field, and the effects of measurement position relative to antiresonances in the response field. As well as providing direct measurements of dynamic stress at a selected location, the measurement methods presented here may find use for the separate analysis of the dynamic stress and velocity components of intensity when undertaking structural intensity measurements. The main limitation of finite differencing methods for the measurement of dynamic stress is that they cannot be used at the boundaries of a system where maximum dynamic stress usually occurs [1].

2. FINITE DIFFERENCING FORMULATIONS

The strain–displacement relation for flexural vibration of a thin beam is

$$\xi(x,t) = -z\frac{\partial^2 w(x,t)}{\partial x^2}, \tag{1}$$

where $\xi(x,t)$ is the strain of a fibre at distance z from the neutral axis, $w(x,t)$ is the transverse displacement, t is the time and x is the axial position along the beam. Maximum dynamic strain occurs at the outermost fibre, distance z_m from the neutral axis, and is given by

$$\xi(x,t) = -z_m\frac{\partial^2 w(x,t)}{\partial x^2}. \tag{2}$$

Equation (2) shows that dynamic bending strain is directly proportional to beam curvature, where the beam curvature is a second order spatial derivative of the continuous displacement function $w(x,t)$. Since only discrete vibration measurements of displacement are possible using vibration transducers such as accelerometers, the second order derivative in equation (2) must be reexpressed in terms of the displacement at discrete locations x_i. Finite differencing approximations are used for this purpose.

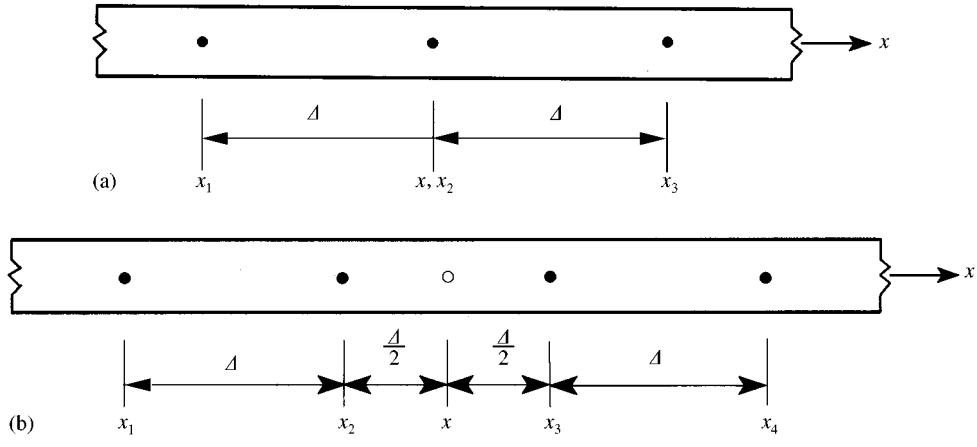

Figure 1. Measurement array for finite differencing: (a) three-point finite differencing; (b) four-point finite differencing.

2.1. THREE-POINT FINITE DIFFERENCING

Substituting the three-point finite differencing approximation for a second-order derivative into equation (2) yields

$$\xi(x,t) = -z_m\left(\frac{w(x_3,t) - 2w(x_2,t) + w\,(w_1,t)}{\Delta^2}\right), \tag{3}$$

where x is the location at which dynamic strain is predicted, Δ is the transducer spacing, and $w(x_i,t)$ is the displacement at position x_i and time t. The measurement positions x_i are symmetric about x as shown in Figure 1(a), and are defined by $x_1 = x - \Delta$, $x_2 = x$ and $x_3 = x + \Delta$. The span over which measurements are performed is 2Δ.

2.2. FOUR-POINT FINITE DIFFERENCING

The four-point finite differencing formulation for dynamic bending strain is

$$\xi(x,t) = -z_m\left(\frac{w(x_4,t) - w(x_3,t) - w(x_2,t) + w(x_1,t)}{2\Delta^2}\right). \tag{4}$$

The measurement positions x_i are symmetric about x and are defined by $x_1 = x - 3\Delta/2$, $x_2 = x - \Delta/2$, $x_3 = x + \Delta/2$ and $x_4 = x + 3\Delta/2$. The spatial extent of the four-point measurement aray is 3Δ. The measurement positions for four-point finite differencing are shown diagrammatically in Figure 1(b).

3. MEASUREMENT METHODS

Measurement methods for finite differencing predictions of dynamic bending strain are derived either directly in the time domain or indirectly in the frequency

domain. The frequency-domain methods are derived using either spectral density functions or frequency response functions, together with the Fourier transform of equation (3) or equation (4). The resulting measurement methods are classified as (a) time-domain differencing, (b) spectral differencing and (c) frequency response function differencing. Methods (a) and (c) can be used for autospectral, spatial and time history predictions of dynamic strain, whereas method (b) only provides autospectral predictions of dynamic strain. The relative advantages of the time- and frequency-domain approaches for this type of application are discussed by Verheij [3]. Frequency response function differencing is used to reduce the number of simultaneous measurements from three or four to only two. Frequency response functions are used by Linjama and Lahti [5] for finite differencing measurements of structural intensity.

3.1. TIME-DOMAIN FINITE DIFFERENCING

Time-domain finite differencing involves the direct evaluation of equation (3) or equation (4) using the simultaneously measured displacements at three or four equally spaced positions. The most practical approach for implementation of time-domain finite differencing is to use an electronic circuit for analogue differencing of the measured displacements. Rearranging equation (3) in terms of first-order differences gives

$$\xi(x,t) = \frac{-z_m}{\Delta^2}\{[w(x_3,t) - w(x_2,t)] - [w(x_2,t) - w(x_1,t)]\} \tag{5}$$

which involves the calculation of three differences at two levels from three inputs. The first two differences are $[w(x_3,t) - w(x_2,t)]$ and $[w(x_2,t) - w(x_1,t)]$, and the third difference is the difference of these two subcalculations. This calculation is implemented electronically using the logic shown in Figure 2(a). Similarly, for four-point finite differencing, equation (4) becomes

$$\xi(x,t) = \frac{z_m}{2\Delta^2}\{[w(x_4,t) - w(x_3,t)] - [w(x_2,t) - w(x_1,t)]\}. \tag{6}$$

In this case there are four inputs, two level of differencing and three differences to be calculated. This calculation is implemented electronically using the logic shown in Figure 2(b).

Since equations (5) and (6) are a linear function of the displacements, either velocity or acceleration may be used in place of displacement as the input signal to the analogue differencing circuit. If the velocity $v(x,t)$ is used as the input signal, dynamic strain for three-point differencing is given by

$$\xi(x,t) = \left(\frac{-z_m}{\Delta^2}\right)\left\{\int_{-\infty}^{\infty}\frac{1}{\mathrm{i}2\pi f}\left(\int_{-\infty}^{\infty} V_{3pt}(x,t)\mathrm{e}^{-\mathrm{i}2\pi ft}\,\mathrm{d}t\right)\mathrm{e}^{\mathrm{i}2\pi ft}\,\mathrm{d}f\right\}, \tag{7}$$

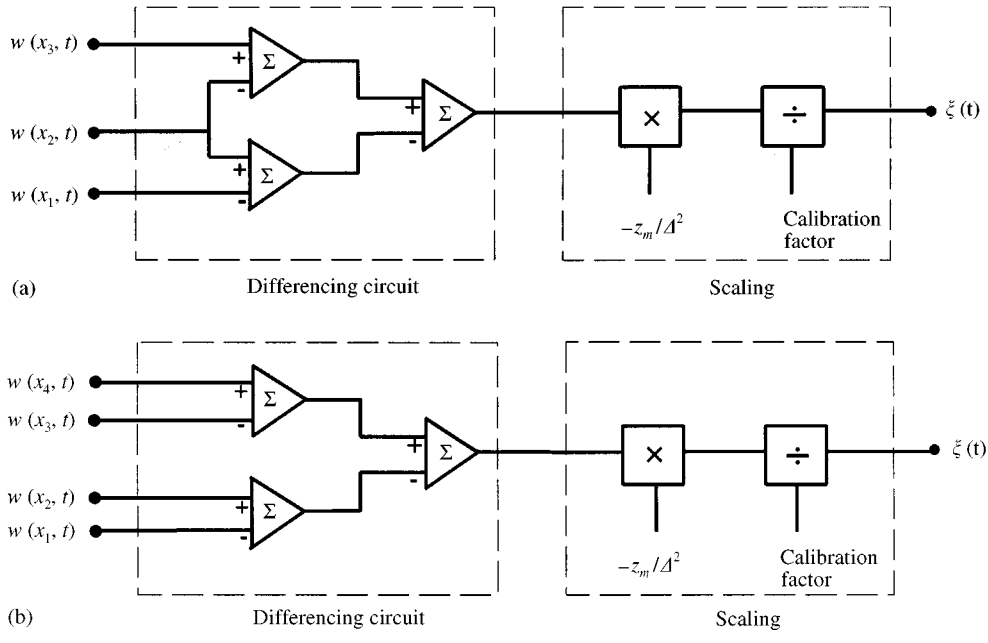

Figure 2. Analogue differencing circuit logic: (a) three point finite differencing; (b) four-point finite differencing.

where

$$V_{3pt}(x,t) = [v(x_3,t) - v(x_2,t)] - [v(x_2,t) - v(x_1,t)] \tag{8}$$

is the output of the three-point analogue differencing circuit. The dynamic strain for four-point differencing using velocity as the input signal is given by

$$\xi(x,t) = \left(\frac{-z_m}{2\Delta^2}\right)\left\{\int_{-\infty}^{\infty}\frac{1}{\mathrm{i}2\pi f}\left(\int_{-\infty}^{\infty} V_{4pt}(x,t)\mathrm{e}^{-\mathrm{i}2\pi ft}\,\mathrm{d}t\right)\mathrm{e}^{\mathrm{i}2\pi ft}\,\mathrm{d}f\right\}, \tag{9}$$

where

$$V_{4pt}(x,t) = [v(x_4,t) - v(x_3,t)] - [v(x_2,t) - v(x_1,t)] \tag{10}$$

is the output of the four-point analogue differencing circuit. Velocity is the preferred vibration signal for time-domain finite differencing since it has a flat frequency weighting which gives the best signal-to-noise ratio over a broad frequency range. If acceleration is used in place of velocity in equations (8) and (10), the factors $1/\mathrm{i}2\pi f$ in equations (7) and (9) are simply replaced by $-1/(2\pi f)^2$. The integrations in equations (7) and (9) are implemented either directly, using an analogue integrator, or indirectly using Fourier transforms, convolution and numerical integration in the complex frequency domain.

3.2. AUTOSPECTRAL PREDICTIONS USING TIME-DOMAIN FINITE DIFFERENCING

Autospectral predictions of dynamic strain using time-domain finite differencing are given by

$$G_{\xi}(x,f) = \langle \bar{\xi}^{*}(x,f)\,\bar{\xi}(x,f)\rangle, \tag{11}$$

where $\bar{\xi}(x,f)$ is the complex Fourier transform of the predicted dynamic strain $\xi(x,t)$ (obtained using time-domain finite differencing), the asterisk denotes the complex conjugate and the brackets $\langle\ \rangle$ are used to denote ensemble averaging. Assuming that velocity is used as the input signal for analogue differencing, substitution of the predicted dynamic strain from equation (7) or equation (9) into the definition for the autospectral density function, equation (11), yields

$$G_{\xi\xi}(x,f) = \left(\frac{z_m}{2\pi f \Delta^2}\right)^2 G_{VV,\,3pt}(x,f) \tag{12}$$

for three-point analogue differencing, and

$$G_{\xi\xi}(x,f) = \left(\frac{z_m}{4\pi f \Delta^2}\right)^2 G_{VV,\,4pt}(x,f) \tag{13}$$

for four-point analogue differencing, where $G_{VV}(x,f)$ is the measured autospectrum of the output signal from the analogue differencing circuit. In this case, the required integrations are performed numerically in the real frequency domain and it is not necessary to use Fourier transform methods and convolution as in section 3.1.

3.3. SPECTRAL FINITE DIFFERENCING

Spectral finite differencing methods for autospectral predictions of dynamic strain are derived by substituting the Fourier transforms of equations (3) and (4) into the definition for the autospectral density function given by equation (11). The Fourier transform of equation (3) for three-point finite differencing is given by

$$\bar{\xi}(x,f) = \left(\frac{-z_m}{\mathrm{i}2\pi f \Delta^2}\right)[\bar{v}_3(f) - 2\bar{v}_2(f) + \bar{v}_1(f)], \tag{14}$$

and the Fourier transform of equation (4) for four-point finite differencing is given by

$$\bar{\xi}(x,f) = \left(\frac{-z_m}{\mathrm{i}4\pi f \Delta^2}\right)[\bar{v}_4(f) - \bar{v}_3(f) - \bar{v}_2(f) + \bar{v}_1(f)], \tag{15}$$

where $\bar{v}_i$ is the Fourier transform of the velocity at position x_i in the transducer array. Substituting these equations into equation (11) yields

$$G_{\xi\xi}(f) = \left(\frac{z_m}{2\pi f \Delta^2}\right)^2 (G_{11}(f) + 4G_{22}(f) + G_{33}(f) + 4\mathrm{Re}\{\mathbf{G}_{12}(f)\} + 2\mathrm{Re}\{\mathbf{G}_{13}(f)\} + 4\mathrm{Re}\{\mathbf{G}_{23}(f)\}) \quad (16)$$

for three-point finite differencing, and

$$G_{\xi\xi}(f) = \left(\frac{z_m}{4\pi f \Delta^2}\right)^2 (G_{11}(f) + G_{22}(f) + G_{33}(f) + G_{44}(f) + 2[\mathrm{Re}\{\mathbf{G}_{14}(f)\} + \mathrm{Re}\{\mathbf{G}_{12}(f)\} - \mathrm{Re}\{\mathbf{G}_{13}(f)\}) + \mathrm{Re}\{\mathbf{G}_{23}(f)\} - \mathrm{Re}\{\mathbf{G}_{24}(f)\} - \mathrm{Re}\{\mathbf{G}_{34}(f)\}] \quad (17)$$

for four-point finite differencing. In the above equations, $G_{\xi\xi}(f)$ is the predicted dynamic strain autospectrum, $G_{ii}(f)$ is the velocity autospectrum for position x_i in the transducer array, and $\mathrm{Re}\{\mathbf{G}_{ij}(f)\}$ is the real part of the complex cross-spectrum between the velocity at position x_i and the velocity at position x_j. These spectral methods require the simultaneous measurement of autospectra at all measurement positions as well as cross-spectra between each combination of measurement positions.

3.4. FREQUENCY RESPONSE FUNCTION FINITE DIFFERENCING

Frequency response function finite differencing can be used to reduce the number of simultaneous measurements required for finite differencing from three or four to only two. The predictions are performed using finite differencing of the frequency response functions measured at each position in the measurement array. The frequency responses are measured sequentially using a roving transducer and a reference, or simultaneously using transducers at each measurement position. Dynamic strain frequency response function predictions obtained using frequency response function finite differencing can be used for time history, autospectral and spatial predictions of dynamic strain.

Methods for the prediction of dynamic strain frequency response functions using measured velocity frequency response functions are derived by substituting the Fourier transform of the dynamic strain finite differencing equation, equation (14) or equation (15), into the definition of the dynamic strain frequency response function given by

$$\mathbf{H}_{R\xi}(x,f) = \frac{\langle \bar{\mathbf{R}}^*(f)\, \bar{\bar{\xi}}(x,f) \rangle}{\langle \bar{\mathbf{R}}^*(f)\, \bar{\mathbf{R}}(f) \rangle}, \quad (18)$$

where $\bar{\mathbf{R}}(f)$ is the complex Fourier transform of the arbitrary reference signal $R(t)$ and $\bar{\xi}(x,f)$ is the complex Fourier transform of the predicted dynamic strain $\xi(x,t)$. Substituting equation (14) for three-point finite differencing into equation (18) gives

$$\mathbf{H}_{R\xi}(x,f) = \left(\frac{z_m}{\mathrm{i}2\pi f \Delta^2}\right)\left(\frac{\langle \bar{\mathbf{R}}^*(f)\bar{v}_3(f)\rangle - 2\langle \bar{\mathbf{R}}^*(f)\bar{v}_2(f)\rangle + \langle \bar{\mathbf{R}}^*(f)\bar{v}_1(f)\rangle}{\langle \bar{\mathbf{R}}^*(f)\bar{\mathbf{R}}(f)\rangle}\right). \tag{19}$$

Since $\mathbf{H}_{Rv_i}(f) = \langle \bar{\mathbf{R}}^*(f)\bar{v}_i(f)\rangle / \langle \bar{\mathbf{R}}^*(f)\bar{\mathbf{R}}(f)\rangle$, equation (19) simplifies to

$$\mathbf{H}_{R\xi}(x,f) = \left(\frac{z_m}{\mathrm{i}2\pi f \Delta^2}\right)(\mathbf{H}_{Rv_3}(f) - 2\mathbf{H}_{Rv_2}(f) + \mathbf{H}_{Rv_1}(f)), \tag{20}$$

where $\mathbf{H}_{Rv_i}(f)$ is the frequency response function between the stationary reference R and the velocity at position x_i in the finite differencing measurement array. Similarly, for four-point finite differencing, the predicted dynamic strain frequency response function is given by

$$\mathbf{H}_{R\xi}(x,f) = \left(\frac{z_m}{\mathrm{i}4\pi f \Delta^2}\right)(\mathbf{H}_{Rv_4}(f) - \mathbf{H}_{Rv_3}(f) - \mathbf{H}_{Rv_2}(f) + \mathbf{H}_{Rv_1}(f)). \tag{21}$$

These results show that finite differencing predictions of dynamic strain can be implemented directly in the frequency domain using finite differencing of measured complex frequency response functions. The above equations are based on the use of velocity measurements, but displacement and acceleration can also be used as outlined in Section 3.1. Since the differencing operations are evaluated numerically, there is no noise introduced during differencing and it is not important whether displacement, velocity or acceleration is used.

3.4.1. *Autospectral predictions*

Autospectral predictions of dynamic strain are calculated from the magnitude of the predicted dynamic strain frequency response function and the measured reference autospectrum $\mathrm{G}_{RR}(f)$ according to

$$\mathbf{G}'_{\xi\xi}(x,f) = |\mathbf{H}_{R\xi}(x,f)|^2\,\mathrm{G}'_{RR}(f). \tag{22}$$

3.4.2. *Spatial predictions*

Spatial distributions of dynamic strain are obtained by repeating autospectral predictions of dynamic strain at various positions along the structure. These autospectral predictions are calculated from the predicted dynamic strain frequency response functions for each position x_1 and a single reference autospectrum $\mathrm{G}'_{RR}(f)$:

$$\mathrm{G}'_{\xi\xi}(x_i,f) = |\mathbf{H}_{R\xi}(x_i,f)|^2\,\mathrm{G}'_{RR}(f). \tag{23}$$

The prime is used to denote the response for the period of the reference measurement $\mathbf{G}'_{RR}(f)$ which is independent of any particular frequency response function measurement $\mathbf{H}_{R\xi}(x_i, f)$. Obviously, the same reference location must be used throughout.

3.4.3. *Time history predictions*

Dynamic strain time histories are predicted using the complex dynamic strain frequency response function $\mathbf{H}_{R\xi}(x, f)$, a time history measurement of the reference and a combination of Fourier transform methods and convolution:

$$\xi(x,t) = \left\{ \int_{-\infty}^{\infty} \mathbf{H}_{R\xi}(x,f) \left(\int_{-\infty}^{\infty} R(t) \mathrm{e}^{-\mathrm{i}2\pi ft} \mathrm{d}t \right) \mathrm{e}^{\mathrm{i}2\pi ft} \mathrm{d}f \right\}. \tag{24}$$

3.5. COMPARISON OF METHODS

The relative benefits of the different methods for practical predictions of dynamic strain depend mainly on the equipment available for performing measurements and the quality of this equipment.

Time-domain finite differencing using an analogue differencing circuit provides a single-channel real-time dynamic strain vibration signal but requires (i) simultaneous measurements at three or four positions; (ii) phase-matched transducers; (iii) phase-matched instrumentation; (iv) a low-noise differencing circuit and (v) accurately calibrated transducers and instrumentation.

Frequency response function finite differencing using transducers at each measurement position can be used to obtain the same information as time-domain finite differentiating without the need for a differencing circuit. This requires a data acquisition system with accurately calibrated simultaneous sampling across three or four channels (if a remote reference is used, the number of transducers is increased by one). These predictions have the same requirements as time-domain finite differencing except that the introduction of noise during the differencing operation is eliminated. If the frequency response measurements are performed sequentially with a roving transducer then the requirements for (i) simultanious measurements at three or four positions, (ii) phase-matched transducers and instrumentation and (iii) accurately calibrated measurement channels are eliminated. Only a two-channel data acquisition system is required for sequential frequency response measurements and the measurement channels do not need to be phase-matched (provided that the phase errors remain constant).

Spectral differencing has the same requirements as frequency response function finite differencing using simultaneous measurements at each measurement position, but is limited to autospectral predictions of dynamic strain.

4. ERROR SOURCES IN FINITE DIFFERENCING PREDICTIONS

Errors in finite differencing predictions of dynamic strain result from (i) finite differencing bias errors, (ii) experimental errors, (iii) statistical errors in

measurements and (iv) measurement noise. Finite differencing bias errors are inherent in the use of finite differencing methods. Statistical errors, experimental errors and measurement noise are of increased significance to the accuracy of finite differencing measurements of dynamic strain due to the sensitivity of the differencing calculations to errors in the data used for differencing. These sources of error must be minimized when performing vibration measurements.

4.1. FINITE DIFFERENCING BIAS ERRORS

Finite differencing bias errors are introduced as a result of using finite differencing approximations for the second order derivative in equation (2). The finite differencing bias error ratio ε is defined by

$$\xi' = \xi\varepsilon, \tag{25}$$

where

$$\varepsilon = \frac{\mathrm{d}^2 w/\mathrm{d}x^2}{\delta^2 w/\delta x^2}, \tag{26}$$

ξ' is the exact dynamic strain, ξ is the predicted dynamic strain and δ is the differencing operator. Equation (25) can be used to account for finite differencing bias errors if the bias error ratio ε is known.

4.1.1. *Propagating wave bias error ratio*

Finite differencing bias errors for propagating waves are derived by evaluating equation (26) for $w(x, k) = \mathbf{A}\mathrm{e}^{\mathrm{i}kx}$. For three-point finite differencing the bias error ratio ε is given by

$$\varepsilon_{3pt} = \frac{-k^2\Delta^2}{\mathrm{e}^{\mathrm{i}k\Delta} - 2 + \mathrm{e}^{-\mathrm{i}k\Delta}} = \frac{k^2\Delta^2}{4\sin^2(k\Delta/2)}, \tag{27}$$

whilst for four-point finite differencing the bias error ratio is

$$\varepsilon_{4pt} = \frac{-k^2\Delta^2}{\mathrm{e}^{\mathrm{i}3k\Delta/2} - \mathrm{e}^{-\mathrm{i}k\Delta/2} - \mathrm{e}^{-\mathrm{i}k\Delta/2} + \mathrm{e}^{-\mathrm{i}3k\Delta/2}} = \frac{k^2\Delta^2}{\cos(k\Delta/2) - \cos(3k\Delta/2)}. \tag{28}$$

The same equations result for two propagating waves moving in opposite directions.

The finite differencing bias error ratios associated with propagating waves for both three- and four-point finite differencing are plotted as a function of wavenumber in Figure 3, using Δ/λ as the abscissa. These errors result in dynamic strain being underpredicted and are a function of wavelength and transducer spacing. The errors are negligible at low frequency but increase with frequency, and are larger for four-point differencing than for three-point differencing. At higher frequencies not shown in Figure 3, as $\Delta/\lambda \to 1$ for three-point differencing and as $\Delta/\lambda \to 0.5$ for four-point differencing, the bias error ratio increases to infinity due to spatial aliasing, limiting the frequency range of predictions. In order to minimize

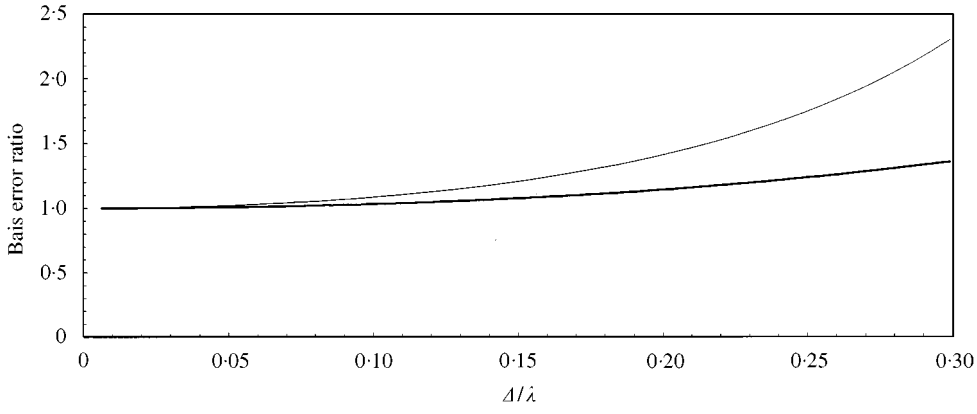

Figure 3. Finite differencing bias error ratio for propagating waves (—— three point differencing; -- four-point differencing).

finite differencing bias errors, and maximize the frequency range of predictions, a small transducer spacing should be used.

4.1.2. *Evanescent wave bias error ratio*

The finite differencing bias error ratio for an evanescent wave in the absence of propagating waves is derived by evaluating equation (26) for $w(x,k) = \mathbf{A}e^{kx}$. For three-point finite differencing the bias error ratio is

$$\varepsilon^1_{3pt} = \frac{k^2\Delta^2}{e^{k\Delta^2} - 2 + e^{-k\Delta}} = \frac{k^2\Delta^2}{2(\cosh(k\Delta) - 1)}, \tag{29}$$

and for four-point finite differencing the bias error ratio is

$$\varepsilon^1_{4pt} = \frac{k^2\Delta^2}{e^{3k\Delta/2} - e^{k\Delta/2} - e^{k\Delta/2} + e^{3k\Delta/2}} = \frac{k^2\Delta^2}{(\cosh(3k\Delta/2) - \cosh(k\Delta/2)}. \tag{30}$$

The bias error ratios from equations (29) and (30) for an evanescent wave were plotted in Figure 4. These errors cause the components of dynamic strain associated with evanescent waves to be overpredicted. Bias errors for evanescent waves are larger for four-point finite differencing than for three-point finite differencing and increase continuously with frequency. The bias error ratios for propagating and evanescent waves are different in terms of both direction and magnitude.

4.1.3. *Correction factors for finite differencing bias errors*

The bias error ratios for propagating waves can be used as a correction factor for finite differencing predictions of dynamic strain to obtain exact predictions in farfield regions and conservative predictions in nearfield regions. This involves scaling finite differencing predictions by equation (27) or equation (28). Exact

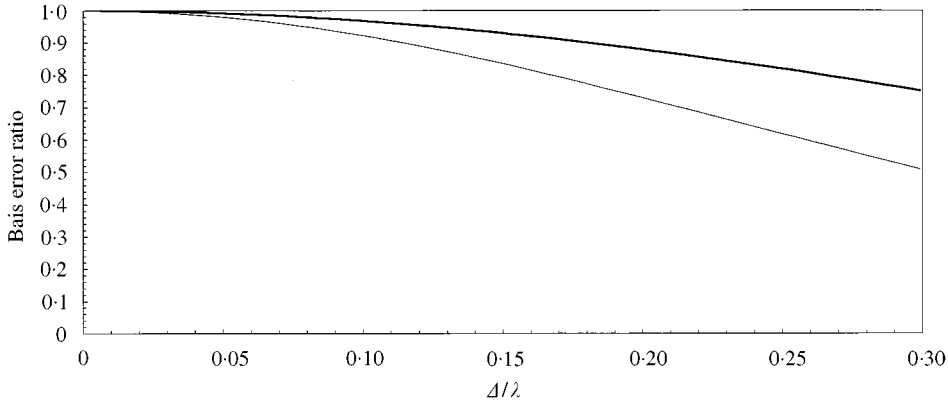

Figure 4. Finite differencing bias error ratio for evanescent waves (—— three point differencing; —— four-point differencing).

predictions in the near field are not possible since the bias error ratios for propagating and evanescent waves are different, and the relative significance of propagating and evanescent waves cannot be pre-determined. The bias error ratio for propagating waves gives conservative predictions in the nearfield since only propagating wave bias errors decrease predicted dynamic strain.

4.2. EXPERIMENTAL ERRORS

Finite differencing calculations are sensitive to factors that produce amplitude errors in the quantities to be differenced. Amplitude errors may result from calibration errors (direct amplitude errors), positioning error (the response amplitude at a different position is used), phase differences (the response amplitude at a different instant is used) and external noise (direct amplitude errors). Assuming that the magnitudes of the errors are frequency independent and a constant transducer spacing is used, finite differencing is most sensitive to experimental errors at low frequency where wavelengths are largest. The reason for this is that the errors as a percentage of the differences being calculated are much larger at low frequency than at high frequency due to the relative closeness of the measurement positions. In order to minimize the sensitivity of predictions to experimental errors, the transducer spacing used should be maximized within the constraints imposed by finite differencing bias errors.

4.3. STATISTICAL ERRORS

Statistical errors will be present in measured autospectra, cross-spectra and frequency response functions. These errors may be random or bias errors, and are described in detail (with formulas for their estimation) by Bendat and Piersol [6]. Statistical random and bias errors produce amplitude errors with the same effects as the experimental errors described in section 4.2.

The most important points for finite differencing predictions are that (i) the resolution bandwidth must be sufficiently small to avoid frequency resolution bias errors; (ii) the number of averages should be large to minimize random errors; (iii) the signal amplitude of measurements should be maximized and (iv) extraneous noise in measurements must be minimized. Finite differencing predictions of dynamic strain are most sensitive to these errors at low frequency and transducer spacing should be maximized (within the constraints imposed by finite differencing bias errors) to minimize the sensitivity of predictions to statistical errors.

5. LIMITATIONS WITH THE FINITE DIFFERENCING METEHOD

The main limitation of finite differencing methods is that they cannot be used to predict dynamic strain at system boundaries. This is due to (i) the spatial extent of the transducer array and (ii) the prediction of dynamic strain at the centre of the transducer array only. Since maximum dynamic strain occurs at the boundaries of systems with one or more clamped boundaries, and the magnitude of dynamic strain decreases rapidly with distance from a clamped boundary, finite differencing cannot be used to directly measure maximum dynamic strain in systems with one or more clamped boundaries.

Other limitations with finite differencing methods are that they are not exact in nearfield regions and they only provide predictions at discrete locations. However, the measurements are easily repeated at a number of locations to obtain a spatially distributed set of predictions for dynamic strain.

6. EXPERIMENTS

Experimental results are presented in this section to demonstrate the use of finite differencing methods for the prediction of dynamic strain autospectra, spatial distributions and time histories. Results demonstrating the application of finite differencing methods to the prediction of dynamic bending strain in a flat plate structure are also presented.

6.1. EXPERIMENTAL PROCEDURES

Finite differencing predictions of dynamic strain were performed for the clamped beam system in Figure 5 and the clamped plate system in Figure 6. Dynamic strain was predicted at each location where strain gauges were installed (Table 1) and compared with the strain gauge measurement of dynamic strain at that location. The finite differencing methods tested were (i) three-point frequency response differencing, (ii) three-point analogue differencing (differencing performed in the time domain) and (iii) four-point frequency response differencing.

6.1.1. *Instrumentation*

The phase-matching characteristics of the B&K 4375 accelerometers used for measurements are summarized in Table 2. These accelerometers were used with

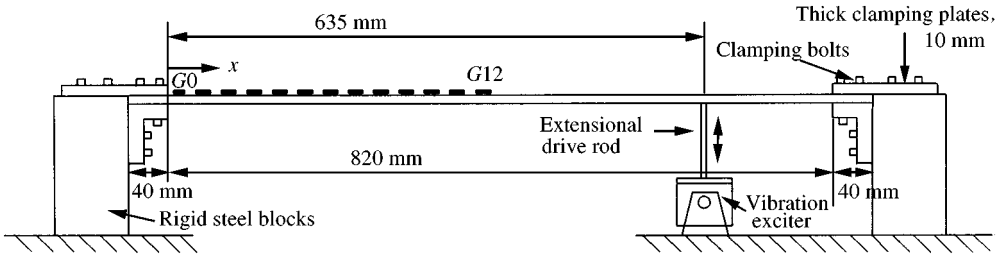

Figure 5. Clamped beam experimental arrangement.

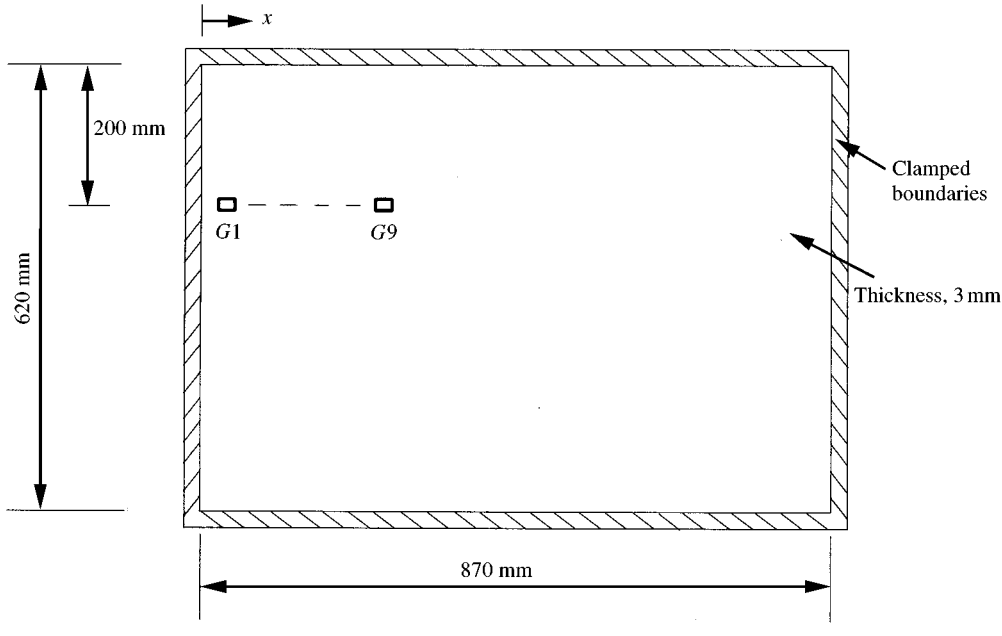

Figure 6. Clamped plate experimental arrangement.

B&K 2636 phase-matched charge amplifiers to obtain velocity vibration signals from the accelerometers and amplify the vibration signal in order to obtain an optimal signal-to-noise ratio over a broad frequency range and minimize the effects of noise present in the differencing circuits. Analogue differencing was performed using a custom-built analogue differencing circuit with the logic shown in Figure 2(a).

6.1.2. *Data processing*

Time history data was measured with a B&K 2133 Real-Time Frequency Analyser. These data were processed either internally within the analyser using

TABLE 1

Strain gauge labels and strain gauge positions for the clamped beam

Gauge	Clamped
0	0·007 m
1	0·025 m
2	0·06 m
3	0·095 m
4	0·13 m
5	0·165 m
6	0·2 m
7	0·235 m
8	0·27 m
9	0·305 m
10	0·34 m
11	0·375 m
12	0·41 m

TABLE 2

Phase-matching characteristics of the accelerometers

Frequency (Hz)	Phase error (deg)
20–100	< 1
100–200	$< 0{\cdot}3$
200–300	$< 0{\cdot}2$
Above 300	$< 0{\cdot}1$

digital filtering, or externally on a personal computer using FFT and convolution routines. All measured data for frequency response function predictions was processed with the FFT software.

Frequency response finite differencing time history predictions of dynamic strain obtained from equation (24) were calculated using the predicted dynamic strain frequency response function, a reference time history (measured simultaneously with the strain gauge dynamic strain time history measurement for that location) and FFT-convolution routines. Exactly the same convolution routines, but with the frequency response function set equal to $(1 + \mathrm{i}0)$, were used to numerically integrate time histories in the complex frequency domain for analogue differencing predictions in the time domain (section 3.1) utilizing velocity or acceleration vibration measurements:

$$x(t) = \left\{ \int_{-\infty}^{\infty} \frac{1}{\mathrm{i}2\pi f}(1 + \mathrm{i}0) \left(\int_{-\infty}^{\infty} \dot{x}(t) \mathrm{e}^{-\mathrm{i}2\pi f t} \, \mathrm{d}t \right) \mathrm{e}^{\mathrm{i}2\pi f t} \, \mathrm{d}f \right\}. \tag{31}$$

TABLE 3

Parameters for signal processing of measurements

	Autospectral predictions	Spatial predictions
Minimum frequency (HP filtering)	20 Hz	20 Hz
Minimum frequency (LP filtering)	1·41 Hz	355 Hz
Nyquist frequency	2048 Hz	512 Hz
Bandwidth	4 Hz	2 Hz
Averages	100	100

Autospectral and spatial predictions of dynamic strain utilizing the FFT routines were processed using the parameters listed in Table 3. A narrow bandwidth was used to minimize bandwidth bias errors and to provide high-resolution results. Time history predictions were measured using a sampling rate of 4096 samples per second and were integrated numerically in the complex frequency domain as described above. For autospectral predictions using analogue differencing and digital filtering, the measured and predicted dynamic strain autospectra were measured simultaneously to 10 kHz in 1/12th octaves.

6.2. EFFECTS OF TRANSDUCER SPACING

Transducer spacing affects the sensitivity of predictions to experimental errors at low frequencies, the magnitude of finite differencing bias errors at mid to high frequencies, and the upper frequency limit of predictions (due to spatial aliasing). The ratios of predicted to measured mean-square dynamic strain for three different transducer spacings were calculated to observe the effect of transducer spacing on the accuracy of predictions for the clamped beam experimental rig. These results are plotted in Figure 7 for three-point analogue differencing predictions of dynamic strain at $x = 0{\cdot}095$ m. The transducer spacings tested were $\Delta = 30$, 40 and 50 mm. As the transducer spacing is increased, low-frequency errors decrease but high-frequency errors increase. Conversely, as the transducer spacing is decreased, low-frequency errors increase but high-frequency errors decrease. These results show that a large transducer spacing is required to minimize the effects of experimental errors at low frequencies, whilst a small transducer spacing is required to minimize the effects of finite differencing bias errors at high frequencies, although the latter can be corrected by scaling predictions using the finite differencing bias error ratio within the confines on upper frequency imposed by spatial aliasing. A transducer spacing of 40 mm was used for all finite differencing predictions of dynamic strain except for the three-point spatial predictions of dynamic strain for which a transducer spacing of 60 mm was used.

6.3. AUTOSPECTRAL PREDICTIONS

In this section, finite differencing autospectral predictions of dynamic strain at locations where strain gauges were installed are compared with the strain gauge

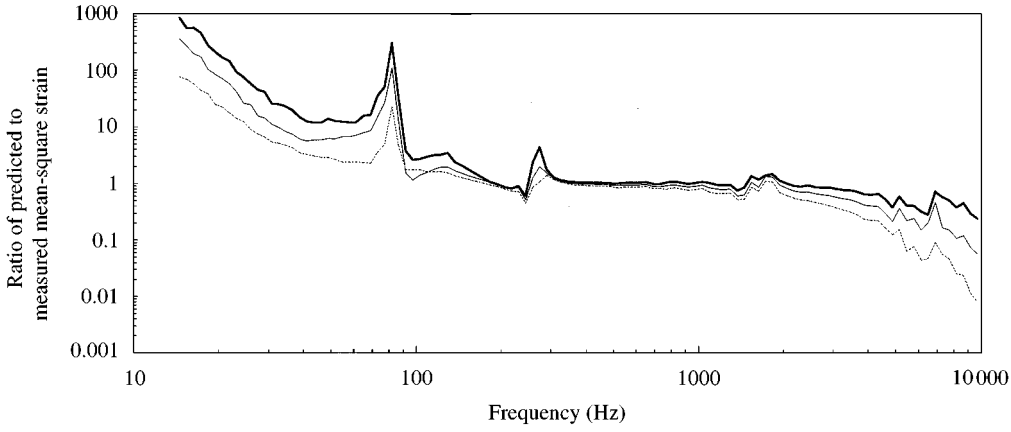

Figure 7. Ratio of finite differencing prediction of dynamic strain to strain gauge measured dynamic strain for three-point analogue differencing (——30 mm transducer spacing; —— 40 mm transducer spacing: - - - 50 mm transducer spacing).

measurement at that location. The predicted dynamic strain autospectra have been scaled by the propagating wave finite differencing bias error ratio to compensate for finite differencing bias errors [refer equations (27) and (28)]. Compensation factors for evanescent wave finite differencing bias errors were not necessary since these errors result in conservative predictions.

6.3.1. *Farfield predictions*

Measured and predicted dynamic strain autospectra for the positions $x = 0{\cdot}235$ and 0·34 m of the clamped beam system are plotted in Figure 8. Predicted dynamic strain autospectra are presented for three-point frequency response differencing, three-point analogue differencing and four-point frequency response differencing.

The predictions overpredict at the first resonant frequency. This is due to finite differencing methods being most sensitive to experimental errors at low frequency and decreased phase matching between accelerometers below 100 Hz. At frequencies above the first resonant frequency, the predicted dynamic strain for each method agrees well with the measured dynamic strain. If correction factors for finite differencing bias errors had not been applied the predictions would have increasingly underpredicted the measured dynamic strain at frequencies above $\sim$ 500 Hz. The observed differences between measured and predicted dynamic strain at anti-resonant frequencies are associated with either (i) the noise floor of the strain gauge measurement system or (ii) the finite length of the strain gauge which prevents measurement of dynamic strain at a discrete point.

Coherence functions and acceleration autospectra are plotted in Figure 9 for the frequency response function measurements used to obtain the three-point frequency response differencing prediction of dynamic strain at $x = 0{\cdot}235$ m in Figure 8(a). Each of the three frequency response measurements of acceleration have frequencies of low coherence corresponding to antiresonances in the

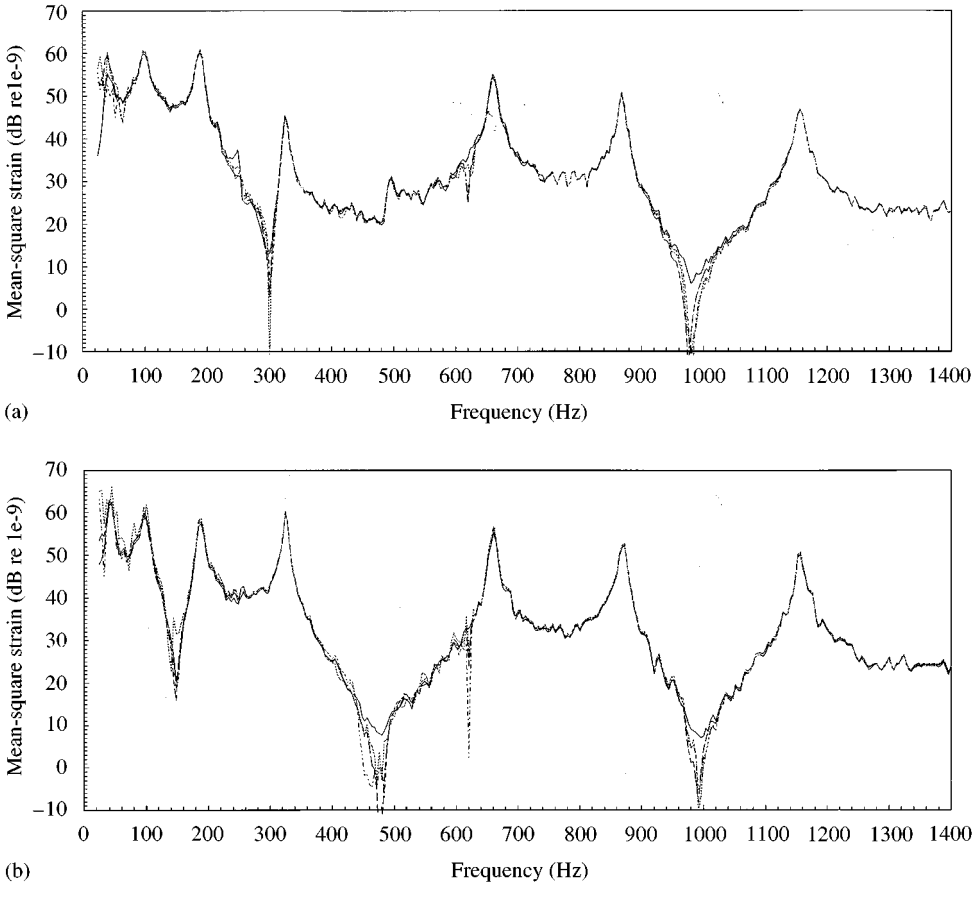

Figure 8. Measured and predicted dynamic strain autospectra in the farfield region of a clamped beam excited at $x = 0{\cdot}635$ m by white noise. (–– measured; - - - three-point frequency response differencing; – – – three point analogue differencing; — - — four-point frequency response differencing); (a) $x = 0{\cdot}095$ m; (b) $x = 0{\cdot}235$ m.

acceleration autospectra for the location where the accelerometer measurement was performed. These antiresonances occur at different frequencies for each position in the measurement array and do not appear to affect the accuracy of predictions. The only frequency at which the predictions were affected by low coherence was at 620 Hz. At this frequency, all three frequency response measurements have low coherence due to an antiresonance at the reference measurement position as shown in Figure 9(b). It should also be noted that in spite of the small amplitude of dynamic strain, the agreement between measured and predicted is very good over a dynamic range of 50 dB indicating that the measurements have a low sensitivity to noise levels in typical laboratory equipment.

6.3.2. *Clamped boundary nearfield predictions*

Measured and predicted dynamic strain autospectra are plotted in Figure 10 for the position $x = 0{\cdot}095$ m of the clamped beam system. This position lies in the

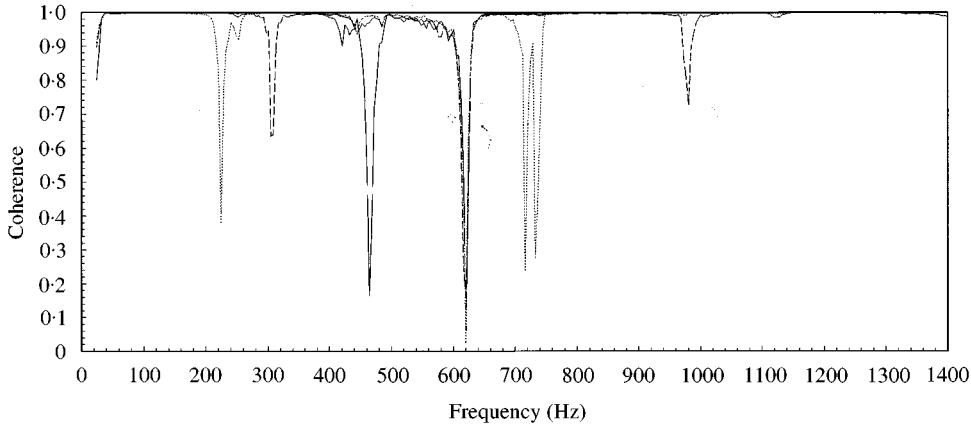

Figure 9(a). Coherence functions for the three-point frequency response prediction of dynamic strain at $x = 0{\cdot}235$ m (—— $x = 0{\cdot}195$ m; – – – $x = 0{\cdot}235$ m; - - - $x = 0{\cdot}275$ m).

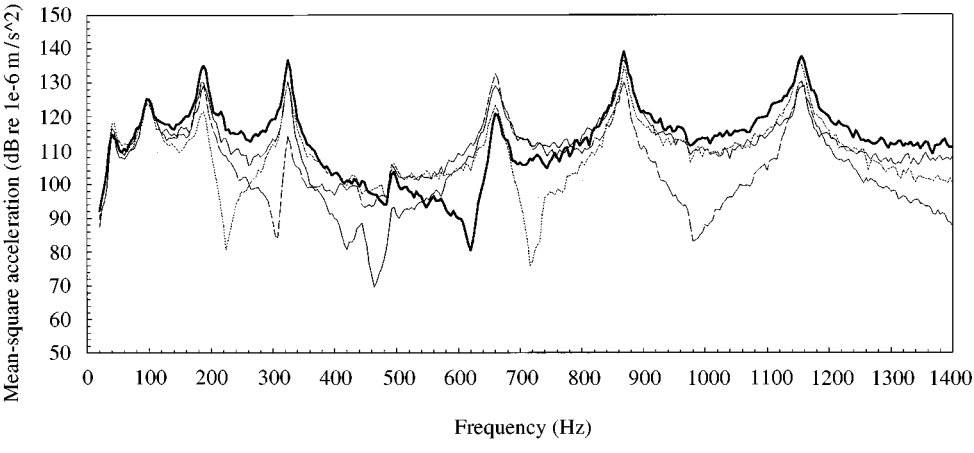

Figure 9(b). Acceleration autospectra for the three-point frequency response prediction of dynamic strain at $x = 0{\cdot}235$ m (—— $x = 0{\cdot}195$ m; – – – $x = 0{\cdot}235$ m; - - - $x = 0{\cdot}275$ m; — reference at $x = 0{\cdot}165$ m).

nearfield region associated with the clamped boundary at frequencies up to 400 Hz. The agreement between measured and predicted dynamic strain is quite good except in the region of the first resonant frequency where the measured dynamic strain is overpredicted. As the agreement between measured and predicted is very good at the second, third and fourth resonant frequencies where the measurement position lies in the near field, these results show that finite differencing can be used for accurate predictions of dynamic strain in nearfield regions.

6.3.3. *Clamped plate*

Measured and predicted dynamic bending strain autospectra at $x = 0{\cdot}125$ m from the boundary of a clamped plate experimental rig are plotted in Figure 11.

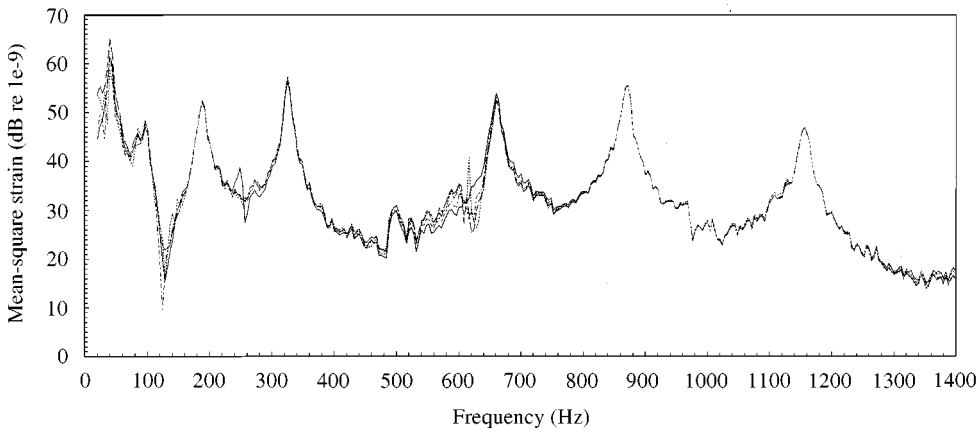

Figure 10. Measured and predicted dynamic strain autospectra at $x = 0{\cdot}095$ m in the clamped boundary nearfield region of a clamped beam excited at $x = 0{\cdot}635$ m by white noise (—— measured; - - - three point frequency response differencing; – – – three point analogue differencing — - — four-point frequency response differencing).

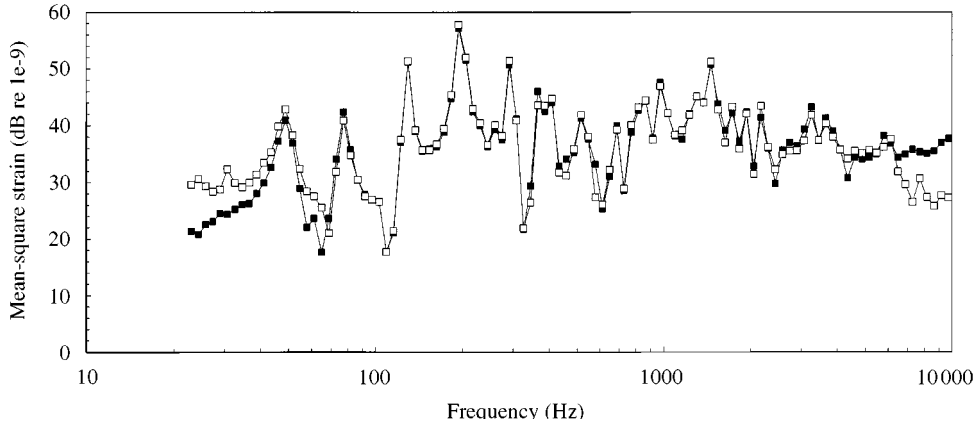

Figure 11. Measured and predicted dynamic strain autospectra at $x = 0{\cdot}125$ m of a clamped plate excited by white noise (—■— measured; —□— predicted).

The predicted dynamic strain was obtained using three-point analogue differencing with a transducer spacing of 40 mm. The agreement between measured and predicted is quite good except for some overprediction of dynamic strain below 100 Hz and above 6 kHz. Nearfield effects do not appear to have influenced the predictions.

6.4. TIME-DOMAIN PREDICTIONS

Time history predictions of dynamic strain using finite differencing methods were performed for the clamped beam system. The predictions presented here were

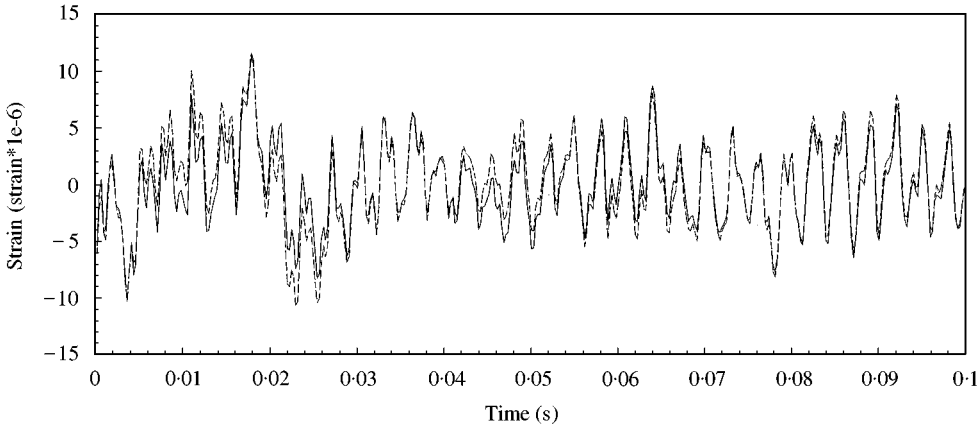

Figure 12. Measured and predicted dynamic strain time histories at $x = 0{\cdot}34$ m of a clamped plate excited at $x = 0{\cdot}635$ m at white noise (—— measured; – – – predicted).

obtained using three-point analogue differencing, but are also representative of three and four-point frequency response finite differencing time history predictions of dynamic strain. The measured data used for these predictions had a lower frequency limit of 20 Hz and an upper frequency limit of 1·41 kHz due to high and low-pass filtering, respectively.

6.4.1. *Farfield predictions*

The measured and predicted dynamic strain time histories at $x = 0{\cdot}34$ m of the clamped beam system for broadband excitation are plotted in Figure 12. The agreement between measured and predicted is quite good except for differences between measured and predicted introduced as a result of low-frequency errors identified in Figure 8(b).

To verify that the errors observed in Figure 12 were in fact due to low-frequency errors in the prediction of dynamic strain, the measurements were repeated using band-limited white noise as the excitation signal. The excitation signal had a centre frequency of 800 Hz and a bandwidth of 400 Hz. The measured and predicted dynamic strain time histories for narrow-band excitation are plotted in Figure 13. There is very good agreement between measured and predicted in this case.

6.4.2. *Nearfield predictions*

The predicted dynamic strain time history at $x = 0{\cdot}06$ m in the clamped boundary nearfield region of the clamped beam experimental rig is compared with the measured dynamic strain for the same location in Figure 14. The beam was excited using broad-band white noise and the predicted dynamic strain time history was obtained using three-point analogue differencing. There is reasonable agreement between the measured and predicted time histories. Errors in the predicted time history are the result of significant low-frequency experimental errors.

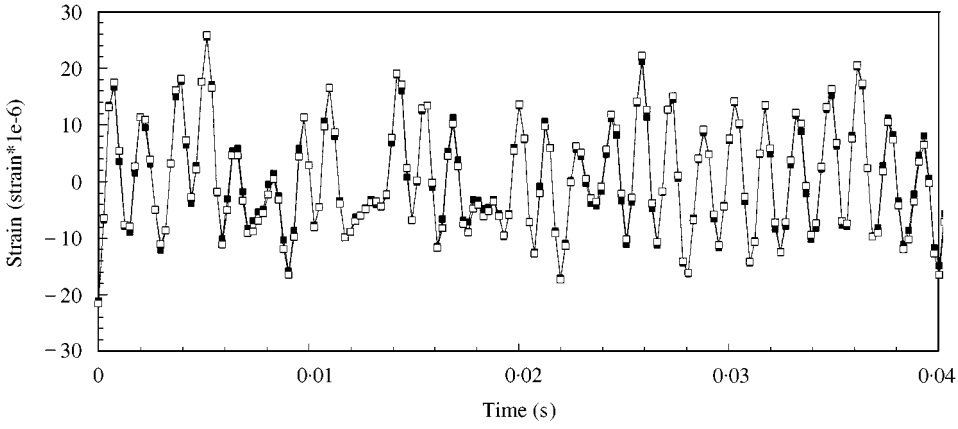

Figure 13. Measured and predicted dynamic strain time histories at $x = 0{\cdot}34$ m of a clamped beam excited at $x = 0.635$ m by band-limited White noise with centre frequency 800 Hz and bandwidth 400 Hz (—■— measured; —□— predicted).

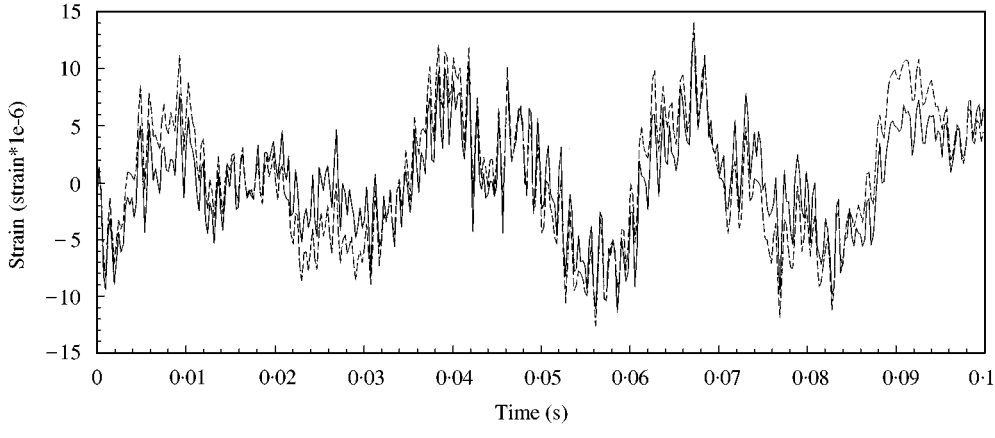

Figure 14. Measured and predicted dynamic strain time histories at $x = 0{\cdot}06$ m of a clamped beam excited at $x = 0{\cdot}635$ m by white noise (—— measured; – – – – predicted).

6.5. SPATIAL PREDICTIONS

The measured and predicted dynamic strain spatial distributions for the first three resonant frequencies of the clamped beam experimental rig are plotted in Figure 15. The finite differencing predictions were obtained using three-point frequency response differencing, three-point analogue differencing and four-point frequency response differencing. Strain–velocity correlation predictions of dynamic strain, obtained using the farfield correlation ratio [1] are also included in Figure 15 for comparison and to identify the farfield and nearfield response regions (the farfield strain–velocity correlation prediction of dynamic strain equals the measured dynamic strain in farfield regions).

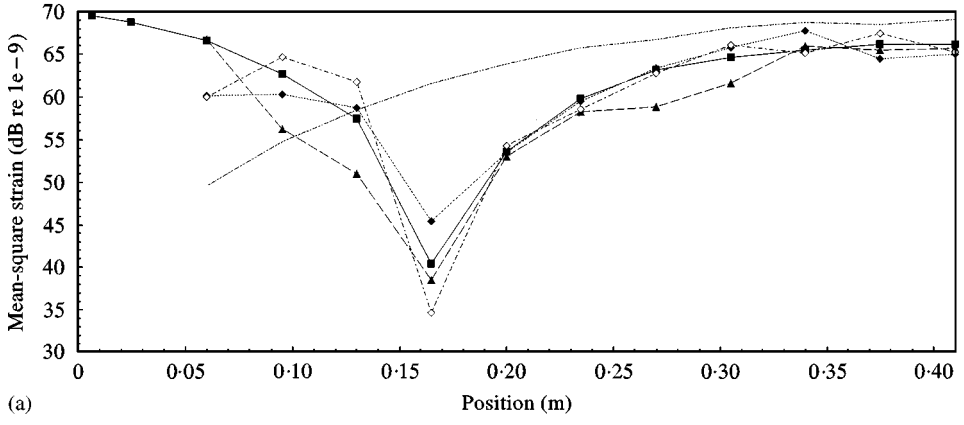

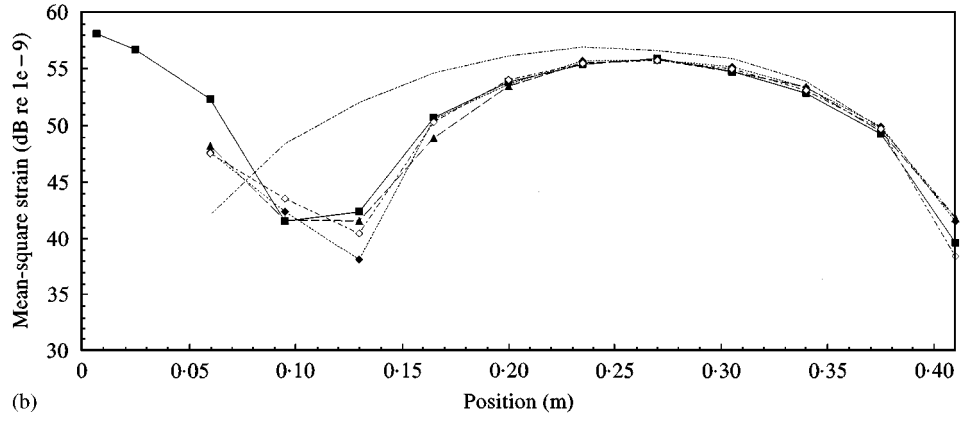

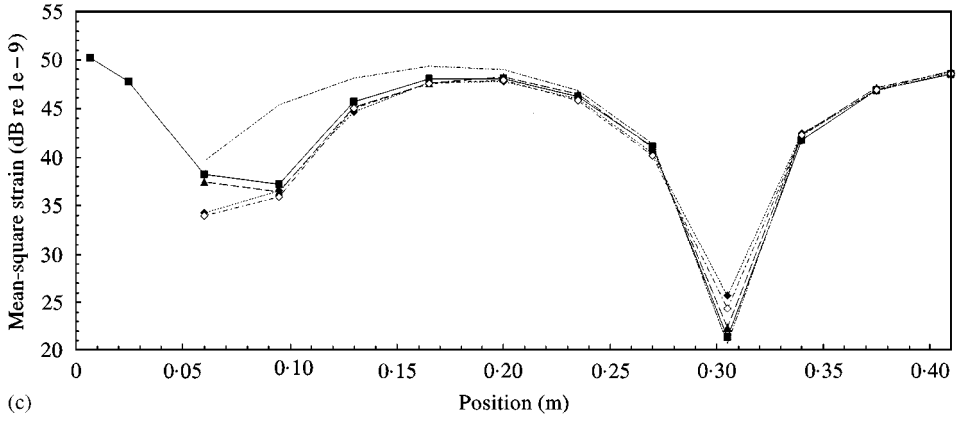

Figure 15. Measured and predicted dynamic strain spatial distributions of a clamped beam excited at $x = 0{\cdot}635$ m by white noise (—■— measured; —▲— three-point frequency response differencing; —◇— three point analogue differencing; —◆— four-point frequency response differencing; — - — strain–velocity correlation). (a) 42 Hz (first natural frequency), (b) 94 Hz (second natural frequency), (c) 185 Hz (third natural frequency).

The finite differencing predictions of dynamic strain are inaccurate in the region of the clamped boundary at the first resonant frequency. Further from the clamped boundary, the predictions are reasonably accurate except for some larger errors in the three-point frequency response differencing predictions at $x = 0{\cdot}27$ and $0{\cdot}305$ m. Inaccuracies in the finite differencing predictions at the first resonant frequency are the result of a high sensitivity to experimental errors (such as positioning errors and phase errors resulting from cable motion) at large wavelengths. The dynamic strain predictions at the second and third resonant frequencies are much more accurate but still underpredict at the position closest to the clamped boundary.

The accuracy of the predictions is seen to be independent of whether dynamic strain is being predicted in the nearfield or the farfield, with correlations between dynamic strain and velocity being limited to the farfield. The nearfield extends from $x = 0{\cdot}0$ to $0{\cdot}35$ m in Figure 15(b) and $x = 0{\cdot}25$ m in Figure 15(c).

The results in Figure 15 show that spatial distributions of dynamic bending strain can be obtained using finite differencing methods. These predictions are independent of whether dynamic strain is being predicted in the near field or far field. However, due to the spatial extent of the transducer array, dynamic strain could not be predicted close to the clamped boundary where dynamic strain was largest. Farfield correlations between dynamic strain and velocity provide equally accurate predictions of dynamic strain at a point in the farfield, but cannot be used to predict dynamic strain in the near field.

7. CONCLUSIONS

Finite differencing formulations for the measurement of dynamic bending strain as derived in this paper provide autospectral, and time history predictions bending strain in both nearfield and farfield regions. These predictions are performed using either time or frequency-domain measurements of the vibrational response. The methods require the simultaneous measurement of displacement or velocity at three or four equally spaced positions. The number of simultaneous measurements required is reduced to two if the response is stationary and frequency response finite differencing is used.

Experimental results demonstrating finite differencing predictions of dynamic bending strain are presented in this paper. Autospectral, spatial and time history predictions of dynamic bending strain, obtained using the finite differencing method, agree well with strain gauge measurements except for errors at the first resonant frequency. These predictions were scaled by the finite differencing bias error ratio for propagating waves to obtain more accurate predictions at higher frequencies.

Finite differencing predictions of dynamic bending strain are sensitive to amplitude errors in the vibration signals used for differencing. Sources of amplitude errors include phase errors as these result in the use of amplitude values from the wrong instant in time. Finite differencing is most sensitive to experimental errors at low frequencies where wavelengths are largest and the difference in signal

amplitude between each measurement position is smallest. To minimize the sensitivity of finite differencing to experimental errors, transducer spacing should be maximized within the constraints imposed by finite differencing bias errors and spatial aliasing. Statistical errors (random and bias) produce amplitude errors with the same effects on the accuracy of predictions as experimental errors. The resolution bandwidth, number of averages and signal-to-noise ratio should be optimized to minimize the effects of these errors. Only the signal-to-noise ratio needs to be considered for time-domain finite differencing. Velocity is the preferred vibration signal for time-domain finite differencing predictions of dynamic bending strain since it has a flat frequency weighting which gives it the best signal-go-noise ratio over a broad frequency range.

Finally, antiresonances at the reference position result in low coherence for the frequency response function measurements at each position in the measurement array, leading to inaccurate predictions at the frequencies of these antiresonances. The reference transducer for frequency response function finite differencing should therefore be positioned to avoid antiresonances at frequencies significant to the response. Anti-resonances at the measurement positions result in low coherence but do not appear to have a significant effect on the accuracy of predictions. Attention should still be paid however to avoiding antiresonances at the measurement positions for vibration at frequencies significant to the response.

The results presented here show that finite differencing methods are of use in place of strain gauges and strain–velocity correlations for direct measurements of dynamic bending strain using accelerometers. The benefits of the finite differencing approach over other accelerometer-based techniques (such as the travelling wave solution method [1, 7]) are that (i) post-processing for dynamic strain can be performed within the frequency analyser used to collect the data, (ii) analogue differencing provides real-time measurements of dynamic strain and (iii) the method can be used to measure both components of dynamic strain in thin-plate structures. The main limitation of the finite differencing method is that it cannot be used to predict dynamic bending strain at system boundaries, where dynamic bending strain is usually largest, due to the spatial extent of the transducer array (dynamic strain is only predicted at the centre of the transducer array). Travelling wave solution methods have been developed by Koss and Karczub [7] for autospectral and spatial predictions of dynamic strain, and by Karczub [1] for time history predictions of dynamic strain, to overcome this limitation with finite differencing methods and provide accurate predictions of dynamic bending strain at any location along a beam.

REFERENCES

1. D. G. Karczub 1996 *Ph.D. Thesis, The University of Western Australia.* The prediction of dynamic stress and strain in randomly vibrating structures using vibrational velocity measurements.
2. G. Pavic 1976 *Journal of Sound and Vibration* **49**, 221–230. Measurement of structure borne wave intensity. Part 1: formulation of the methods.

3. J. W. Verheij 1980 *Journal of Sound and Vibration* **70**, 133–139. Cross spectral density methods for measuring structure borne power flow on beams and pipes.
4. J. M. Cuschieri 1991 *Noise Control Engineering Journal* **37**, 97–107. Experimental measurement of structural intensity on an aircraft fuselage.
5. J. Linjama and T. Lahti 1992 *Journal of Sound and Vibration* **153**, 21–36. Estimation of bending wave intensity in beams using the frequency response technique.
6. J. S. Bendat and A. G. Piersol 1980 *Engineering Applications of Correlation and Spectral Analysis.* New York: John Wiley.
7. L. L. Koss and D.G. Karczub 1995 *Journal of Sound and Vibration* **184**, 229–244. Euler beam bending wave solution predictions of dynamic strain using frequency response functions.